Local magnetic properties of antiferromagnetic $FeBr_2$

J. Pelloth, R. A. Brand, S. Takele, M. M. Pereira de Azevedo, W. Kleemann, Ch. Binek, and J. Kushauer
Angewandte Physik, Gerhard-Mercator-Universität Gesamthochschule Duisburg, D-47048 Duisburg, Germany

D. Bertrand
Laboratoire de Physique des Solides, associé au CNRS (URA 74) INSA, F-31077 Toulouse, France
(Received 19 June 1995)

The antiferromagnet $FeBr_2$ has been studied by Mössbauer spectroscopy in external fields both in the metamagnetic region below the multicritical temperature T_{MCP} and in the second-order transition region above. The local magnetization shows that the metamagnetic transition occurs by spin flips, as in simple models. However, in the second-order transition region, the local magnetization of the sublattice oriented antiparallel to the external field varies continuously but remains parallel to the c axis. This can only be understood if the external magnetic field induces strong transversal spin precession of the moments on the antiparallel sublattice. This shows that the anomalous maxima in the imaginary part χ'' recently found in the ac susceptibility [M.M. Pereira de Azevedo *et al.*, J. Magn. Magn. Mater. **140-144**, 1557 (1995)] and denoted H_- below the critical field $H_C(T)$, and H_+ above, can be understood as being caused by noncritical transversal spin fluctuations.

I. INTRODUCTION

Compounds of transition metal halogens have been intensively studied as model systems for antiferromagnets (AF) with strong uniaxial anisotropy. Both $FeCl_2$ and $FeBr_2$ have attracted special attention. The AF magnetic order in these two compounds can be described as an antiferromagnetic stacking of ferromagnetic (FM) layers. They show a first-order metamagnetic phase transition at low temperature in external magnetic field parallel to the c-axis. Above a certain multicritical point, the transition becomes continuous, and second-order. In the past, the chloride compound has attracted more interest because of the lower external fields required for the metamagnetic transition. In this work, we concentrate on the metamagnet $FeBr_2$, which shows qualitatively similar behavior as $FeCl_2$, but with large quantitative differences. The most important difference is an unusual form of the second-order critical field H_C–temperature T phase line above the multicritical point (MCP) with $T_{MCP}=4.64$ K.[1] The critical behavior in the neighborhood of T_{MCP} has not been explained as yet. It has been shown[2] that because of the unusual form of the phase line, this probably ends in a critical endpoint (CEP), and not in a more usual tricritical point (TCP). The critical behavior in the neighborhood of external field $H_a=0$, and T about equal to the Néel temperature $T_N=14.2$ K is unusual. Here, the measured specific heat[3] is much larger than that which would be predicted from the critical exponent α, where in zero field $1.32\leqslant\alpha\leqslant 1.56$. It should be mentioned in this context that recent neutron-diffraction studies[4] have shown that the intraplane correlation length ξ does not diverge at T_N. The properties of the spin waves have received much attention in $FeBr_2$. The spin wave dispersion curves have been studied by several groups[5,6] in order to determine the different exchange and anisotropy interactions important in this system.

Recently the ac susceptibility has been studied[7] both for the first-order metamagnetic transition below T_{MCP}, and the second-order continuous transition above T_{MCP} but below T_N. It was found that in the continuous transition region the real part χ' has a maximum at the critical line in field, $H_C(T)$, but not the imaginary part χ''. Instead, the imaginary part shows a local minimum, and maxima both below and above this field, denoted as H_- and H_+, respectively. In addition, the derivative of the total magnetization M with respect to the temperature T, dM/dT, at constant field, and with respect to field dM/dH at constant T, was also found to display maxima below the critical line $H_C(T)$ at H_-. Figure 1 shows the phase diagram of $FeBr_2$ taken from Ref. 7. The lines in the figure separate the different phase regions: AF, (saturated) paramagnetic (PM), and the mixed phase region (AF+PM). These are taken from $M(H_a)$ at constant T and $M(T)$ at constant H_a as well as $dM(T)/dT$ measurements. The second-order continuous critical field line H_C separates the AF and PM regions above $T_{MCP}=4.64$ K. The other points, given by χ' and χ'' as a function of T and H_a yield H_- below H_C, and H_+ above. The bars around these points denote the regimes of strong noncritical fluctuations.[7] It can be seen from this figure that both these regimes, that within the ordered phase with maximum at H_-, and the other in the PM phase with maximum at H_+ seem to merge at the multicritical point $H_C(T_{MCP})$.

The anomalies in the ac and total magnetization of $FeBr_2$ were originally attributed to the competing interactions along the in-plane axes of the triangular Fe lattice planes.[7] Recent Monte Carlo simulations[8] reinforce this view. Moreover, they revealed that the large number of equivalent superexchange paths between adjacent Fe^{2+} layers is crucial to fully explain the anomalies. Interestingly, the same result has recently been found within the framework of an infinite-dimensional Hubbard model using quantum-Monte-Carlo techniques.[9] The presence of these anomalies, and the vanishing of the imaginary part of the ac susceptibility at the critical line leads to the hypothesis that there are transverse in addition to the longitudinal fluctuations in-

0163-1829/95/52(21)/15372(15)/$06.00

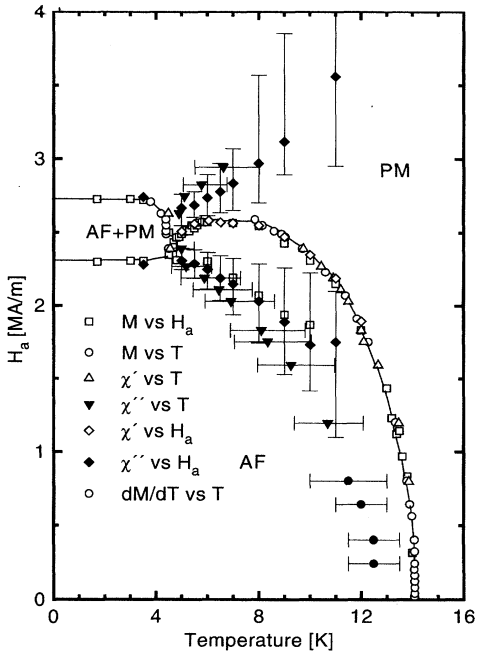

FIG. 1. The magnetic phase diagram $H_a(T)$ of $FeBr_2$ where H_a is the applied field (taken from Ref. 7). The eye-guiding lines separate the different phase regions: antiferromagnetic (AF), (saturated) paramagnetic (PM), and the mixed phase region (AF+PM) as given by the $M(H_a)$ at constant T and $M(T)$ at constant H_a as well as $dM(T)/dT$ measurements. The second-order continuous critical-field line H_C separates the AF and PM regions above $T_{MCP}=4.64$ K. The other points, given by χ' and χ'' as a function of T and H_a are discussed in the text, and yield H_- below H_C, and H_+ above. The bars around these points represent the width of the maxima, and not error bars.

volved in this transition. For this reason, we have made an extensive ^{57}Fe Mössbauer study of the magnetic transitions in temperature and field using a part of the same single crystal as was used by Pereira de Azevedo *et al.*[7] Our goal was to obtain better understanding of the local magnetization in the continuous transition range. Our results show clearly that the metamagnetic transition proceeds by spin flips of 180° in a mixed phase region. Along the second-order critical line, the transition is different. There is a continuous change in the local moments of mainly the antiparallel sublattice. They from $-g_{\|}\mu_B$ to $+g_{\|}\mu_B$ continuously, remaining parallel to the c axis ($g_{\|}=g$ factor parallel to c axis; μ_B = Bohr magneton). This variation is over a field range that agrees well with the characteristic fields H_- and H_+ as derived from the ac susceptibility and total magnetization. This variation is a direct consequence of the transverse noncritical fluctuations on the antiparallel sublattice induced by the external field in the presence of the competing exchange interactions.

This paper is divided in the following way. The crystal-field and spin-orbit coupling are discussed in Sec. II with respect to the magnetic phase diagram. Hyperfine effects are discussed in Sec. III. The experimental studies using ^{57}Fe Mössbauer spectroscopy are presented in Sec. IV. The review presented in Secs. II and III is necessary for the discussion of these results presented in Sec. V.

II. CRYSTAL-FIELD AND MAGNETIC PROPERTIES OF $FeBr_2$

A. Crystal-field and spin-orbit coupling in $FeBr_2$

It is instructive to discuss the details of the crystal-field splitting in the iron halides in more detail. The magnetic properties of the iron halide crystals FeH_2 (H=Cl,Br,I) have been extensively studied due to their very interesting properties, and these are strongly influenced by the crystal-field splitting. $FeBr_2$ is an ionic crystal with CdI_2 structure, space group $D^3{}_{3d}$ (see Ref. 10). The lattice is hexagonal, with one molecular unit per unit cell. The structure can be described as Fe^{2+} layers that are separated by two Br^- layers, and stacked along the c axis, with lattice constants $a=3.74$ Å, $c=6.17$ Å. The magnetic properties have been studied by Wilkinson *et al.*,[11] and are similar to that of $FeCl_2$. The electronic state of the free high-spin Fe^{2+} ion is ^5D with an electronic configuration of $3d^6$: the total orbital quantum number $L'=2$, and spin quantum number $S'=2$ (see Ref. 12). The local symmetry is cubic with a small trigonal deformation. There are strong ferromagnetic exchange interactions J_1 between the $Z_1=6$ nearest-neighbor (NN) Fe ions within the plane, and much smaller antiferromagnetic superexchange interactions J' between neighboring planes. It was originally assumed that the number of J' interactions is two corresponding to the shortest interlayer distances. However, it was recently observed[22] that there are $Z'=20$ equivalent paths for the J' superexchange interactions. Since the product $Z'J'$ is determined experimentally, the magnitude of J' previously reported must be rescaled. In several different studies, the importance of interactions with next- and third-next-nearest neighbor (NNN and NNNN) within the plane has been indicated. The phonon and magnon spectra of $FeCl_2$ and $FeBr_2$ have been extensively studied using both inelastic neutron diffusion[5,6,13] and Raman scattering[14] and far-infrared absorption spectroscopy.[15] The appropriate crystal-field Hamiltonian has been extensively discussed by Balucani and Stasch.[12] Here we summarize their results. There are strong hybridization effects between the magnetic excitations (magnons) and the lattice excitations (phonons) due to the crystal-field splitting. This leads to anomalies in the phonon spectra as well. The crystal-field effects in Fe^{2+} compounds with respect to Mössbauer spectroscopy have been extensively discussed by Price and Varret.[16]

The Fe^{2+} ground-state triplet in the cubic term of the crystal field leads to the possibility to characterize it as having an effective $L=1$ orbital momentum. This is done conventionally by matching matrix elements of the crystal-field Hamiltonian for the real and for the effective spin operators and is described in Refs. 12 and 16. In the case of the spin-orbit term, this leads to the following replacement: $\Lambda\mathbf{L}'\cdot\mathbf{S}\rightarrow\lambda\mathbf{L}\cdot\mathbf{S}$ where the effective spin-orbit coupling constant $\lambda=-\Lambda\approx 100$ cm^{-1} is often taken, and the effective $L=1$ is opposite in sense to the real $L'=2$. As before, $S'=2$. The trigonal distortion can also be written in terms of this effective L as $\mathscr{H}_{\rm trig}=-\delta(\mathbf{L}_z)^2$ to within an unimportant constant, and δ is proportional to the trigonal distortion. There are now $(2L+1)(2S'+1)=15$ total states to consider, which, however, group into three manifolds centered near the energies of 0, 2λ, and 5λ from the spin-orbit coupling. This allows a description in terms of the effective total

angular momentum $\mathbf{J}=\mathbf{L}+\mathbf{S}'$ or quantum number $J=1$, 2, or 3. Since 2λ is about 200 $cm^{-1} \approx 200$ K, for our purposes here, we can restrict ourselves to the $J=1$ state, sometimes written as the effective spin $S=1$. This state is triply degenerate ($m_S=-1,0,+1$). The effect of the trigonal distortion on this state leads to a lifting of the degeneracy. The state $|S=1,m_S=0\rangle$ lies above the $|S=1,m_S=\pm 1\rangle$ states by the splitting

$$D=\frac{\delta}{10}\left[1+\frac{9}{100}\frac{\delta}{\lambda}\right]. \tag{1}$$

The single-ion Hamiltonian must also include the Zeeman effect. In terms of the real angular momentum operators L' and S', this is written as $\mathscr{H}_Z=-\mu_B\vec{B}\cdot(\mathbf{L}'+\mathbf{S}')$. When this is expressed in terms of the effective spin operators given above, we obtain the anisotropic g factors that are approximately

$$g_{\parallel}\sim\frac{7}{2}+\frac{9}{20}\frac{\delta}{\lambda} \tag{2a}$$

$$g_{\perp}\sim\frac{7}{2}-\frac{9}{40}\frac{\delta}{\lambda}. \tag{2b}$$

If we estimate that $\delta/\lambda\approx 1$, then $g_{\parallel}\approx 3.9$ and $g_{\perp}\approx 3.3$, not too far away from the values reported by Johnstone, Lockwood, and Mischler[17] To linear order in δ/λ, the ratio of $g_{\perp}/g_{\parallel}\approx 1-(27/140)\delta/\lambda$ is equal to about 0.8 for $\delta/\lambda\approx 1$. The Hamiltonian for the exchange terms is written as $\mathscr{H}_E=-2\Sigma_{i,j}J_{ij}\mathbf{S}_i'\cdot\mathbf{S}_j'$. In the space of the effective spin operator $\mathbf{S}$, this is replaced by a sum over $-J_{ij}[A_{\parallel}^2\mathbf{S}_i^z\cdot\mathbf{S}_j^z+A_{\perp}^2\mathbf{S}_i^+\cdot\mathbf{S}_j^-]$. The constants $A_{\parallel}$ and $A_{\perp}$ expressing the asymmetry in the effective exchange constants are given by $A_{\parallel}\sim\frac{3}{2}[1+(1/10)\delta/\lambda]$, and $A_{\perp}\sim\frac{3}{2}[1-(1/20)\delta/\lambda]$. In the same limit as above, $A_{\perp}/A_{\parallel}\approx 1-(3/20)\delta/\lambda$ or about 0.85 for $\delta/\lambda\approx 1$. The J-mixing term δ/λ thus leads to effective Zeeman and exchange terms that are anisotropic. This contributes to the gap in the magnon spectrum.

B. Magnetic phase diagram of $FeBr_2$

Below T_N, there is long-range AF order in zero field. The Fe^{2+} ions are ordered ferromagnetically within the layers, and stacked antiferromagnetically along the c axis. There is a first-order phase transition in external magnetic field parallel to the c axis for temperatures below the multicritical point at $T_{MCP}=4.64$ K and a critical internal field $H_{MCP}=H_C(T_{MCP})$ which is 2.26 MA/m. The high-field state can be described as a saturated paramagnetic (SPM) phase with a ferromagnetic spin texture due to the external field. The phase transition is continuous and of second order for temperatures above T_{MCP} as given in Ref. 1. The boundary point between the first-order metamagnetic and the second-order continuous transition lines was termed a tricritical point by Griffiths and Wheeler.[18] Early models within the mean-field approximation (MFA) have been reviewed by Stryjewski and Giordano.[19] (See as well Kincaid and Cohen,[20] incorrectly referenced in Ref. 19.) The strong uniaxial anisotropy constrains the spins along the c axis and prevents the occurrence of a spin-flop phase. The first-order metamagnetic transition at finite temperatures is possible (within MFA) only in the presence of different exchange interactions acting within and between the magnetic sublattices. To first approximation in $FeBr_2$, these are the J_1 intralayer FM and J' interlayer AF interactions. Within the MFA,[20] the ratio $\mathscr{R}=Z_1J_1/Z'J'$ determines the main features of the magnetic phase diagram. Z_1 (Z') is the number of FM J_1 (AF J') interactions (note the differences in notation as well as AF/FM sign convention from the paper by Stryjewski and Giordano[19]). For $\mathscr{R}<-3/5$, the line of low-temperature first-order transitions ends where it meets the line of second-order transitions at a tricritical point (T_{TCP}). At this point, there is no change in slope. Within the MFA, the ratio $(T_{TCP}/T_N)^{(MFA)}=1+1/(3\mathscr{R})$ (where $\mathscr{R}<0$). It is known that the MFA leads to a predicted transition temperature $k_BT_N^{(MFA)}=(2/3)S(S+1)(Z_1J_1-Z'J')$ (where $J'<0$) which is too high. The values of the exchange interactions (discussed later) lead to predictions for $\mathscr{R}\approx -5$ and $(T_{TCP}/T_N)^{(MFA)}\approx 0.9$. This latter is much larger than the experimental $T_{MCP}/T_N\approx 0.33$. An Ising-spin model was proposed by Harbus and Stanley[21] for the case of antiferromatically coupled ferromagnetic sublattice structures. In this model, it is the existence of the intrasublattice FM interactions which leads to the tricritical behavior, and the predicted ratio T_{MCP}/T_N is only somewhat smaller than the MFA estimation. Both Monte Carlo and random-phase approximations[22] lead to predicted ratios that are also larger than the experimental one (but smaller than the MFA). The calculations presented are based on the dominating exchange interactions J_1 and J'. It is not clear if agreement would be better if further interplane interactions (J_2 and J_3) were also included. In addition, the dipole energies are mostly neglected in these theories, which may not be justifiable in view of the large moments and low transition temperatures. We must conclude that the experimental T_{MCP}/T_N in $FeBr_2$ has never been correctly explained in the simple theories presented. The most remarkable feature of the phase line in $FeBr_2$, not present in $FeCl_2$, is that above T_{MCP} the critical phase line $H_C(T)$ starts with a positive slope so there is break in slope (kink point) in the phase line at the MCP. This also means that starting at internal fields just above H_C at T_{MCP} and heating will lead to first a transition from the SPM, to the AF, and then back to the SPM states. Within the MFA, such a behavior can be predicted for $-3/5<\mathscr{R}<0$. The first estimation of $\mathscr{R}$ by Jacobs and Lawrence[23] was about -0.28 based on T_N and $H_C(T=0)$. However, such a small value for $\mathscr{R}$ is difficult to justify. The values for the exchange constants discussed below and given in Table I lead to $\mathscr{R}\approx -5$. In a series of papers, Onyszkiewicz has tried to explain this feature of the transition in $FeBr_2$ on the basis of a Heisenberg-type spin Hamiltonian including four-spin anisotropy interactions.[24] However, a

TABLE I. Exchange interactions in $FeBr_2$. The interaction J' has been corrected for the number of interactions $Z'=20$ (taken from Ref. 20).

Ref.	J_1/k_B (K)	J_2/k_B (K)	J_3/k_B (K)	J'/k_B (K)	D/k_B (K)
5	9.3	−3.1	not determined	−0.37	10.7
4, 6	6.2	−0.14	−1.3	−0.37	12

proof of the existence of such four-spin anisotropy interactions has never been presented. Only very recently,[9] the peculiar shape of the $FeBr_2$ phase diagram has been realistically mimicked within a Hubbard model of highly correlated electrons. The MCP seems to be the critical endpoint (CE) of the second-order phase line, whereas the first-order line extends up to a bicritical point (BCE). Hence, a new phase boundary between CE and BCE seems to separate two different antiferromagnetic phases just along the ridge of noncritical fluctuations observed experimentally (see Fig. 1).[7] The very existence of a real phase boundary remains to be shown. But the predicted $T_{CE}/T_N \approx 0.28$ is rather close to the experimental $T_{MCP}/T_N \approx 0.33$.

The magnon dispersion relations in $FeBr_2$ have received extensive experimental[25,26] and theoretical[12,27,24] treatments in the literature. There is evidence of strong magnon-magnon as well as magnon-phonon interactions. In an early paper, Yelon and Vettier[5] have derived the magnetic excitations and have found two propagating modes in which the spins are precessing around the c axis. One of these modes is dispersionless and has zero weight at $T=0$ K, but begins to interact with the other, classical spin wave mode, at finite temperature. There is mixing of the modes where they cross in reciprocal space, leading to mode repulsion. Unfortunately here as in the other studies of the spin wave spectrum in $FeBr_2$, no results are presented for the two sublattices individually.

Birgeneau *et al.*[28] using inelastic neutron scattering to study the magnon dispersion relations have shown that in the case of $FeCl_2$, three types of exchange integrals are needed to describe the magnetic excitations. These are denoted as J_1, the NN FM and J_2, the NNN AF intraplane interactions and J', the AF interplane interaction. Yelon *et al.*[5,13] have studied $FeBr_2$, and used a similar scheme. In order to study the low-temperature excitations of the magnetic system, it is not sufficient to use the molecular-field approximation, as it is well known that this approximation misses the spin waves, only considering single spin excitations. The appropriate transformation to Bose spin operators has been given in Balucani and Stasch.[12] The excitation spectrum contains a zero-field gap $\hbar\omega_0$ that depends on the exchange and anisotropy constants. The gap can be measured by far-infrared absorption spectroscopy as well as directly by inelastic neutron scattering. Using the former method, Petitgrand and Meyer[15] have given $\hbar\omega_0 \approx 17.09(6)\ \mathrm{cm}^{-1} \approx 2.1$ meV. Recently, the gap was measured directly, and a value of about 2 meV was also found.[4]

Recent polarized neutron dispersion studies using other crystallographic directions have shown[4] that there is in addition an AF exchange interaction between in-plane third neighbors (NNNN) J_3 as discussed above. The value of this fourth exchange interaction is small. However the increased frustration helps to destabilize the structure of the FM planes, leading to the possibility of new types of magnetic excitations. These will be discussed below with respect to the results. It must also be realized that this will change the estimates for the ratio δ/λ from the magnetic properties. Table I shows a summary of the results for the exchange and anisotropy interactions proposed in the literature. The interplane interaction J' has been corrected for the number of effective interactions $Z'=20$.

III. HYPERFINE EFFECTS

A. Hyperfine magnetic field

In this section we consider the origin of the different contributions to the hyperfine magnetic field (see for example Price and Varret in Ref. 16, or Ref. 29). The magnetic interaction of the nucleus with the local electronic structure can be written in the static effective-field approximation as the hyperfine Hamiltonian:

$$\mathscr{H}_{\mathrm{hf}} = g_N \mu_N \vec{B}_{\mathrm{hf}} \cdot \mathbf{I}, \tag{3}$$

where $\vec{B}_{\mathrm{hf}}$ is the hyperfine field at the nucleus, g_N is the nuclear g factor, μ_N is the nuclear magneton, and $\mathbf{I}$ is the nuclear spin operator. It is convention to report this field as a flux density B rather as a magnetic field H (where $B=\mu_0 H$) since what is measured is an energy splitting in the nucleus and not a macroscopic field. The major contributions to B_{hf} can be written

$$\vec{B}_{\mathrm{hf}} = \vec{B}_c + \vec{B}_d + \vec{B}_o, \tag{4}$$

where B_c is the Fermi contact field, B_d the intraionic dipolar field, and B_o the effective orbital field. B_c is proportional to the magnetic polarization $m(0)$ of the s electrons within a Thompson radius of the nucleus, which in turn is created by the polarization of the s electrons by the moment of (mainly) the d shell: $\vec{B}_c = (8\pi/3)\mu_B \vec{m}(0)$. In general, both core s electrons and the valence $4s$ electrons must be included in this term, and it is common to separate these into core contributions due to the local moment, and transferred hyperfine contributions due to the matrix magnetization. The resulting B_c is negative: B_c is antiparallel to the atomic d-shell magnetic moment because $m(0)$ of the s electrons is antiparallel to the moment μ_{Fe} of the d electrons. B_d is due to the dipolar interaction between the spin part of the atomic magnetic moment and the nucleus. It is $\vec{B}_d = -2\mu_B \langle [3\vec{r}(\mathbf{S}\cdot\vec{r}) - r^2\mathbf{S}]/r^5 \rangle$. Here, $\vec{r}$ denotes the electron position and $\mathbf{S}$ is the electron spin operator. The angular brackets denote an average over the occupied atomic orbitals. For Ising spins, the dipolar term can also be written as $B_d = \mu_B q_S \langle S_z \rangle/2$ where q_s is proportional to the electric field gradient at the nucleus $q_s = \langle (3\cos^2\Theta - 1)/r^3 \rangle$. The intraionic orbital contribution is proportional to the (unquenched) orbital moment. It can be written as $\vec{B}_o = -2\mu_B \langle \mathbf{L}/r^3 \rangle$ where $\mathbf{L}$ is the orbital angular momentum operator. Both B_d and B_o are positive contributions: they have the same direction as the atomic moment. The sign of the resulting effective internal field (in zero external field) depends on the relative magnitudes of B_c and $B_d + B_o$. In metals, the intra- and interionic dipolar fields are usually small (but not negligible). In the case of Fe^{2+}, the orbital contribution is large, resulting in a positive hyperfine constant along the c axis between the field B_{hf} and the iron moment μ_{Fe} as reported by Simkin.[30] In noncubic environments, the hyperfine constant may not be a scalar even within the static-field approximation. In this case, the hyperfine constant $\tilde{\mathbf{A}}_{\mathrm{hf}}$ is a tensor and can be written

$$\vec{B}_{\mathrm{hf}} = \tilde{\mathbf{A}}_{\mathrm{hf}} \cdot \vec{\mu}_{\mathrm{Fe}}. \tag{5}$$

Due to the hexagonal symmetry we can restrict ourselves to two-dimensional vectors $\vec{B}_{\rm hf}$ and $\vec{\mu}_{\rm Fe}$ with components perpendicular ($\perp$) and parallel ($\|$) to the c axis. This is known to be strictly true for the dipole field,[31] and should be adequate for the other quantities here. Then in component form we have:

$$\vec{B}_{\rm hf}=\begin{pmatrix} B_{\rm hf\perp} \\ B_{\rm hf\|} \end{pmatrix}, \tag{6a}$$

$$\tilde{\mathbf{A}}_{\rm hf}=\begin{pmatrix} a_{\rm hf\perp} & 0 \\ 0 & a_{\rm hf\|} \end{pmatrix}, \tag{6b}$$

$$\vec{\mu}_{\rm Fe}=\mu_B\begin{pmatrix} g_\perp \sin\Theta_\mu \\ g_\| \cos\Theta_\mu \end{pmatrix}. \tag{6c}$$

The magnetic moments $\mu_{\rm Fe}$ make an angle Θ_μ with the c axis. The anisotropy of the hyperfine coupling constant is mainly created by the dipolar B_d and orbital B_o contributions since they reflect the deviation from spherical symmetry of the atomic orbitals. Thus the resulting hyperfine field is no longer parallel to the direction of the magnetic moments except in the case of alignment along the c axis, or in the a-b plane. In this case we must determine two components of $a_{\rm hf}$ in order to calculate moment directions. This effect is known to be present in several fluosilicates,[32] but there is no experimental determination of $a_{\rm hf\perp}$ in $FeBr_2$. Mishra *et al.*[33] have studied numerically the isomer shift and hyperfine field for molecular $FeCl_2$ and $FeBr_2$. The predicted hyperfine fields are very anisotropic, depending on the direction of the magnetic moment with respect to the molecular axis, and this effect is mainly due to changes in the dipolar contributions. Similar effects may occur in the solids. However, they predict negative hyperfine constants for the molecules, while it is known for $FeBr_2$, parallel to the c axis, that it is positive.[30] Unfortunately they were not aware of the work of Simkin (or of Fujita, Ito, and Ôno[34]) on the solids.

In addition, we must include the effect of the applied external magnetic field $H_a=B_{\rm ext}/\mu_0$ [$\mu_0=4\pi/10$ T/(MA/m)] as well as the interionic dipole fields B_D leading to the effective field $B_{\rm eff}$ at the angle $\Theta_{\rm eff}$ that we can also divide into an internal $B_{\rm int}$ and an external field $B_{\rm ext}$:

$$\vec{B}_{\rm eff}=\vec{B}_{\rm int}+\vec{B}_{\rm ext}. \tag{7}$$

The internal field is composed of the hyperfine field defined in Eq. (4) and the interionic dipole field:

$$\vec{B}_{\rm int}=\vec{B}_{\rm hf}+\vec{B}_D. \tag{8}$$

In the case of a finite homogeneously magnetized sample, it is usual to write the interionic dipole field B_D in terms of the demagnetizing field B_1, the Lorenz field B_2, and a remaining dipole field B_3 (for example, see Ref. 35):

$$\vec{B}_D=\vec{B}_1+\vec{B}_2+\vec{B}_3. \tag{9}$$

$\vec{B}_1$ and $\vec{B}_2$ are given by the magnetization $\vec{M}$ while $\vec{B}_3$ is given by an infinite sum over dipole fields:

$$\vec{B}_1=-\tilde{N}_D\mu_0\vec{M}, \tag{10a}$$

$$\vec{B}_2=+\frac{1}{3}\mu_0\vec{M}, \tag{10b}$$

$$\vec{B}_3=\frac{\mu_0}{2\pi}\sum_i^\infty \frac{3(\vec{\mu}_i\cdot\vec{r}_i)\vec{r}_i-r_i^2\vec{\mu}_i}{r_i^5}. \tag{10c}$$

μ_i is the ith Fe moment at position $\vec{r}_i$. The effect of a finite sample with nonspherical shape is given by $\vec{B}_1+\vec{B}_2$. For the sample geometry considered here (flat disk with normal parallel to the crystallographic c axis), the demagnetizing tensor $\tilde{N}_D$ in the idealized case has a value of 1 for magnetization $\vec{M}$ parallel to the c axis, and zero for $\vec{M}$ in the a-b plane:

$$\tilde{N}_D=\begin{pmatrix} 0 & 0 \\ 0 & 1 \end{pmatrix}. \tag{11}$$

The dipole sum in B_3 is nonzero for noncubic lattices. In calculating B_3, it is important to include successive spherical shells of ions up to an upper radius, and then check convergence for large radius. Here we can divide B_3 into parts due to the magnetization of the two sublattices individually. The lattice sums involved in B_3 have been recalculated in the point charge approximation. In terms of the in-plane ($\perp$) and c-axis ($\|$) components of the Fe moment, B_3 is given by

$$\vec{B}_3=\vec{B}_3^{(+)}+\vec{B}_3^{(-)}, \tag{12a}$$

$$\vec{B}_3^{(i)}=\begin{pmatrix} B_{3\perp}^{(i)} \\ B_{3\|}^{(i)} \end{pmatrix} \tag{12b}$$

$$=K^{(i)}\left(\frac{\mu_0}{4\pi}\mu_B\frac{N}{V}\right)\begin{pmatrix} g_\perp \sin\Theta_\mu^{(i)} \\ -2g_\| \cos\Theta_\mu^{(i)} \end{pmatrix}. \tag{12c}$$

In this expression, the ion is assumed to be on the sublattice parallel to the positive direction of the c axis (direction of the external field for the parallel field case). The contribution from the "+" planes [$(i)=(+)$ and so from the *same* sublattice] is given by $K^{(+)}=+4.63$; from the "−" planes [$(i)=(-)$: the *other* sublattice], $K^{(-)}=-1.46$. The constant $(\mu_0/4\pi)\mu_B N/V=0.1559$ T for the experimental Fe number density N/V. The saturation moment of Fe^{2+} is $\mu_{\rm Fe}=g_\|\mu_B=3.95\mu_B$ parallel to the c axis. We have used the experimental $c/a=1.650$ in this calculation. From the above, we see that $B_3=B_3^{(+)}+B_3^{(-)}$ can be nonparallel to $\vec{M}$, if $\vec{M}$ has both parallel and perpendicular components. The macroscopic field B_1+B_2 can be written in terms of the perpendicular and parallel components of the moments on the "+" and "−" sublattices which will be useful later for calculations. For our samples (the component of $\tilde{N}_D$ is 0 for the perpendicular, and 1 for the parallel component) this is

$$\vec{B}_1+\vec{B}_2=\frac{1}{6}\mu_0\mu_B\frac{N}{V}\begin{pmatrix} g_\perp(\sin\Theta_\mu^{(+)}+\sin\Theta_\mu^{(-)}) \\ -2g_\|(\cos\Theta_\mu^{(+)}+\cos\Theta_\mu^{(-)}) \end{pmatrix}. \tag{13}$$

(The coefficients 1 and −2 in the components above are the result of the assumed layerlike sample shape and not the hexagonal layer structure as is the case for B_3.) The dipole field B_D will be reduced by the effects of bond covalence

(see for example Owen and Thornley[36]). This covalence is at the same time responsible for the magnetic exchange interactions present here.

Simkin has studied the magnetic hyperfine properties of $FeBr_2$ at $T=4.2$ K in external magnetic field parallel to the c axis.[30] In this study, he showed that the resulting hyperfine fields on the two sublattices change linearly in B_{ext} up to the (external) spin-flip field B_{sf} of 3.17 T, one with an increasing, and one with a decreasing effective field. Above this, there was only one subspectrum detected, with the larger effective field, showing that the hyperfine constant is positive. At fields above B_{sf}, the effective field at the nucleus varied again linearly, but now with an offset towards smaller values. Simkin related this offset to the change in the interionic dipole terms between the case of antiferromagnetic alignment before spin flip, to the ferromagnetic alignment after and estimated this change as -0.67 T (at $T=4.2$ K). Simkin gives the results of a lattice sum over dipole fields that he says yields a prediction of -0.68 T for this change. We have recalculated this and obtain different results, which will be presented below.

B. Electric field gradient (EFG)

In this section, we discuss the effects of the crystal field and spin-orbit levels on the measured electric field gradient (EFG). Generally the EFG is separated into two parts: the intraionic and the lattice (or ligand) contributions. Here we mainly discuss the interionic contribution since this should dominate in the case of Fe^{2+} in noncubic crystals. The quadrupole splitting ΔE_Q in the absence of magnetic ordering is given by the EFG and the quadrupole moment Q of the 3/2 nuclear state:

$$\Delta E_Q=\left|\frac{1}{2}\,e^2 q_{zz} Q\right|\sqrt{1+\frac{\eta^2}{3}}. \tag{14}$$

The q_{zz} is the largest component in magnitude of the EFG tensor (given by $q_{zz}=V_{zz}/e$) and the anisotropy effect η is defined in the usual way (for example, see Srivastava *et al.* in Ref. 16). The total EFG is usually divided into a lattice (l) and an ionic valence (v) contribution $q_{ij}=(1-\gamma_\infty)q_{ij}^{(l)}+(1-R)q_{ij}^{(v)}$. Both the d shell and the neighboring ions distort the core states, leading to the effective Sternheimer shielding factors γ_∞ and R. Literature values for Fe^{2+} ions are $\gamma_\infty\approx -10$ and $R\approx 0.3$ (see Srivastava *et al.* in Ref. 16). Using the electronic occupation for high-spin Fe^{2+} and the evaluation of $q_{zz}^{(v)}$ for $3d$ states (see for example Price and Varret in Ref. 16), we obtain $+(4/7)\langle r^{-3}\rangle_{3d}$ along the c axis, and asymmetry parameter $\eta=0$. The relationship between the lattice contribution and the ionic one is simple only in the case of point charge models. In the case of covalent bonding, no general rules apply.

In an extensive study of the temperature dependence of the EFG ΔE_Q and the central line shift δ(T), Fujita *et al.*[34] showed that ΔE_Q is very dependent on the temperature (as is also the case in $FeCl_2$ and FeI_2). They were able to estimate the crystal-field and spin-orbit parameters from this temperature dependence, using the method proposed by Ingalls.[37] In this method, the electric quadrupole effect is reduced with increasing temperature due to the thermal population of higher crystal-field states. The zero-temperature limit is given by the maximum splitting given by $\Delta E_Q^0=(2/7)e^2\,Q(1-R)\langle r^{-3}\rangle$ where Q is the nuclear quadrupole moment. The temperature dependence of the EFG is given by $\Delta E_Q(T)=\Delta\,E_Q^0\,F(\Delta,\lambda',2Jz,T)$. The reduction factor F is a function of the crystal-field parameter Δ (due to the trigonal distortion), the effective spin-orbit coupling λ', the magnetic interactions $2ZJ$ (Z = number of neighbors), and the temperature T. They found for $FeBr_2$, $\Delta=125$ K, $\lambda'=125$ K, and $2ZJ=4.5$ K. In this calculation, $2ZJ$ represents the combined effect of the J_1 and J' interactions. The calculation was performed in the mean-field approximation and $2ZJ$ was chosen to reproduce a T_N which was thought to be 11 K at that time ($FeBr_2$). Despite these rather strong simplifications, the resulting theoretical curve very accurately reflects the measured $\Delta E_Q(T)$ over a temperature range extending from well below T_N up to over 300 K.[34] However, this approach has several difficulties. The effective spin-orbit coupling parameter λ' depends on the free-ion spin-orbit parameter λ_0 as $\lambda'=\alpha^2\lambda_0$, where α^2 is a covalence factor strongly influencing the value of $\langle r^{-3}\rangle$. In the case of α-$FeSO_4$, it has been possible to apply molecular-orbital calculations including all of the iron valence and the ligand orbitals as a basis set.[38] The effect of an external field on the ΔE_Q value has been calculated by Zimmermann *et al.*[38] from first principles by adding the Zeeman term to the electronic Hamiltonian. The change in ΔE_Q is with a positive slope: with increasing field, the EFG effect increases. This is because of the fact that in a large external field, only one electronic state will be populated. Unfortunately, it has not yet been possible to combine this method with the effects of the magnetic order present at low temperature so that there are strong deviations at low temperature. However, it is still possible to use the same molecular field approximation as in the method of Ingalls.[37] This was also shown by Zimmermann, Trautwein, and Harris.[38] These results are also discussed at length in Ref. 39.

IV. EXPERIMENTAL RESULTS

A. Samples and experiments

Samples of $FeBr_2$ platelets thin enough for Mössbauer spectroscopy have been prepared from the same single crystals reported on previously[7] for the ac-susceptibility studies. They were prepared by pulling off the surface of the crystal on the a-b plane using adhesive tape. The platelets were prepared under inert atmosphere, and sealed in small Plexiglass holders. Spectra have been taken from the single-crystal films. The samples were cooled only once in a magnet cryostat and all measurements taken without returning the sample back to room temperature (zero-field measurements as well). In this way, the samples could be retained without water uptake for long periods in the cryostat. The γ ray was always parallel to the c axis which is the direction of alignment of the moments in the AF phase. For this reason, the nuclear $\Delta m=0$ lines are not seen in zero field. The external magnetic field was either parallel or perpendicular to the γ ray, as noted below. For the experiments in perpendicular field, it was only necessary to rotate the sample in the cryostat.

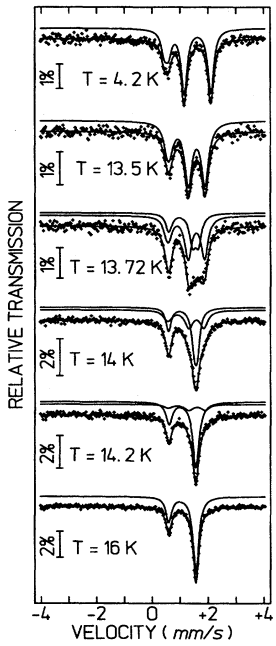

FIG. 2. Mössbauer spectra for increasing temperature in zero external field. Shown are the two-subspectra fits in the neighborhood of T_N as explained in the text.

The Mössbauer spectra were evaluated using a full diagonalization of the ground and excited state static Hamiltonian, and so they include all eight nuclear transitions present for mixed hyperfine effects. All fits have been performed using this type of algorithm. In certain cases, an accurate transmission integral formalism was used for the spectral area but the samples studied here were both well within the thin-absorber approximation, the main problem being the strong absorption of the γ rays by bromine.

B. Mössbauer results

1. Results for zero field: T=4.2 K to above T_N

The spectra in zero external field are shown in Fig. 2 for temperatures from 4.2 to 16 K, well above the $T_N=14.2$ K. The line-area asymmetry for the spectra from the paramagnetic phase (PM), $T>T_N$ shows that the nuclear excited state $m_e=\pm 3/2$ lies above the $m_e=\pm 1/2$ so that the EFG is positive, $q_{zz}>0$, as given above for the ionic contribution, and as determined before.[30,34] Below T_N, the magnetic order is seen as an additional Zeeman splitting, that of the excited state $m_e=\pm 3/2$ being three times faster than that of the other, leading to the apparent three-line spectra. The hyperfine field $B_{\rm eff}$ at $T=4.2$ K is 2.99(1) T, in agreement with previous results.[30,34] (The number in parentheses indicates the uncertainty of the last digit.) For consistency, we will denote the measured hyperfine field by $B_{\rm eff}$, at the angle $\Theta_{\rm eff}$ with respect to the c axis (also γ-ray direction). Even in zero field, $B_{\rm eff}$ must be corrected for the dipole field to arrive at the hyperfine field $B_{\rm hf}$ defined above, and $\Theta_{\rm eff}\equiv 0°$. Figures 3(a) and 3(b) show in detail the variation of $B_{\rm eff}(T)$ and $\Delta E_Q(T)=e^2q_{zz}(T)Q/2$ (where $\eta=0$). Both the multicritical $T_{\rm MCP}$ and Néel T_N temperatures are shown. In the neighborhood of T_N, average values are shown as open symbols. A careful observation of the spectra shown in Fig. 2 shows that just below T_N in a very small temperature interval, two distinct subspectra are visible, one with larger, and one with smaller $B_{\rm eff}$ and ΔE_Q values. This is shown in detail in Figs. 4(a) and 4(b) in the neighborhood of T_N. These values, weighed with the respective subspectra areas, were used for the open symbols in Figs. 3(a) and 3(b). This unexpected behavior will be discussed in Sec. VI. In this temperature region, special care was taken to ensure that the temperature regulation during the measurements was stable to much better than $\pm 0.03°$. Absolute temperature control was to about $\pm 0.1°$. The temperature variation of ΔE_Q has previously been given by Fujita, Ito, and Ôno.[34] There is a variation even in the absence of the magnetic order appearing at T_N. This variation is strongest in the region of $T\approx D\approx \delta/10$ [see Eq. (1)], due to the thermal population into the atomic $m_S=0$ state as discussed above. There is an additional increase in ΔE_Q at decreasing temperatures due to the effect of the magnetic order. The resulting exchange field on the ion lifts the degeneracy of the $m_S=\pm 1$ level and leads to a singlet ground state. It is seen from the discussion above on the EFG splitting that a singlet state leads to the largest ΔE_Q, as has been discussed by Price and Varret in Ref. 16. In Table II, the results for the zero-field spectra are summarized.

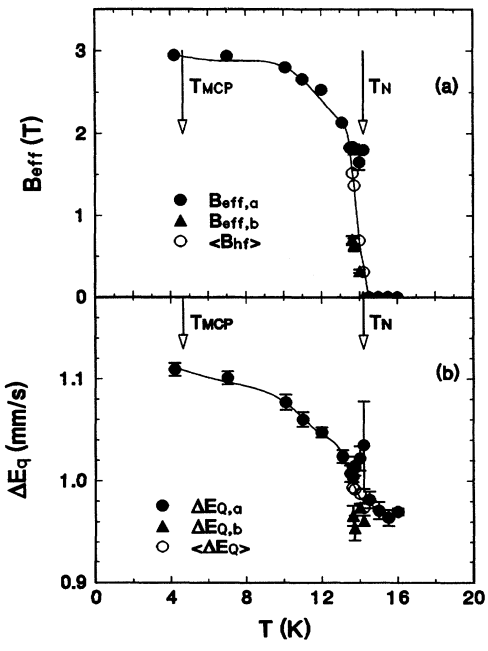

FIG. 3. Results for (a) hyperfine fields $B_{\rm eff}$ (T) and (b) ΔE_Q (T) in zero external field. The multicritical $T_{\rm MCP}$ and Néel T_N temperatures are shown. The open symbols near T_N are for average values from the two subspectra. The results for the two-subspectra fits near T_N are shown in Fig. 4 in greater detail. Lines are guides for the eye.

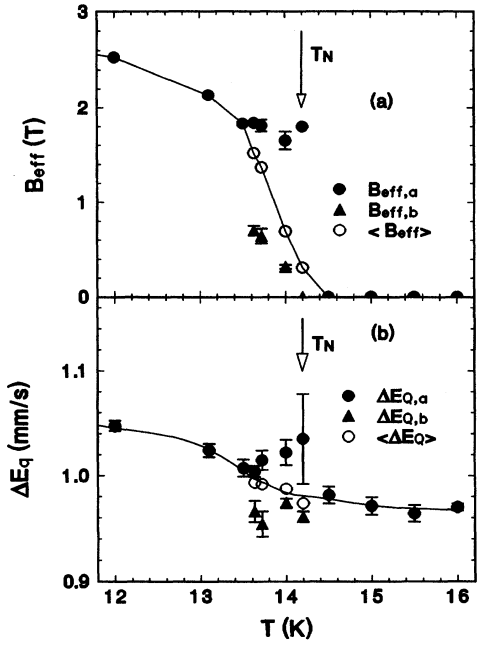

FIG. 4. Results for (a) hyperfine fields B_{eff} (T) and (b) ΔE_Q (T) in zero external field. The multicritical T_{MCP} and Néel T_N temperatures are shown. The open symbols near T_N are for average values from the two subspectra weighted by the relative areas. Lines are guides for the eye.

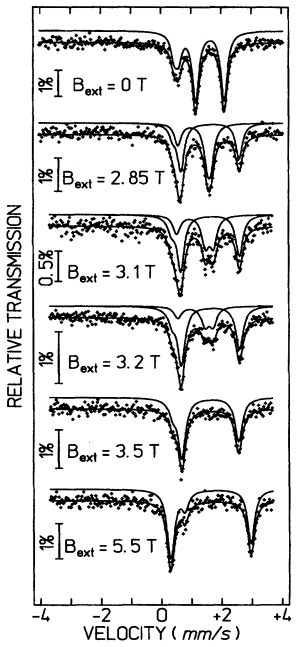

FIG. 5. Mössbauer spectra for $T=4.2$ K, increasing parallel field. Shown are the two-subspectra fits: the measured $B_{\text{eff},a}$ increases with B_{ext}, while the measured $B_{\text{eff},b}$ decreases. This is interpreted as a negative initial value, shifting to positive values with increasing B_{ext}.

2. Results for T=4.2 K in parallel external field: Metamagnetic transition

Typical spectra for $T=4.2$ K in increasing external magnetic field parallel to the c axis are shown in Fig. 5. It is clear that in external field two subspectra are distinguishable, and that the effective hyperfine field B_{eff} increases for one [denoted (a)], and decreases for the other subspectrum [denoted (b)] as seen before.[30] These are shown in Fig. 6(a), starting at $B_{\text{eff}}(4.2\text{ K},0\text{ T})=2.99$ T. $B_{\text{eff},a}$ increases with B_{ext}: in Fig. 6(a), this is compared with the line $B_a=B_{\text{eff},a}$ (4.2 K,0 T) $+B_{\text{ext}}$. The results for $B_{\text{eff},b}$ decrease at first with increasing B_{ext}: these starting values are also shown as *negative* values, compared with the line $B_b=B_{\text{eff},b}$ (4.2 K,0 T)$+B_{\text{ext}}$. The zero-field result is shown as two equal-area subspectra denoted (a) and (b), one with $B_{\text{eff},a}=+2.99$ T, and one with $B_{\text{eff},b}=-2.99$ T. It is known that the sign of the hyperfine field constant along the c axis is positive, consistent with the angular momentum contribution dominant in Fe^{2+} [see Eq.

TABLE II. Results from zero external field, increasing temperature. In the neighborhood of T_N, the division into two subspectra (a) and (b) is given. Γ is the linewidth (full width at half maximum), δ the center shift (isomer shift: with respect to α-Fe at room temperature). Errors are given in parentheses [(0) denotes fixed value].

T (K)	Γ (mm/s)	δ (mm/s)	$\Delta E_{Q,a}$ (mm/s)	$B_{\text{eff},a}$ (T)	A_a (%)	$\Delta E_{Q,b}$ (mm/s)	$B_{\text{eff},b}$ (T)	A_b (%)
4.2	0.260(5)	1.185(3)	1.109(6)	2.95(1)	100(0)	–	–	0(0)
7.0	0.259(7)	1.187(4)	1.101(6)	2.94(1)	100(0)	–	–	0(0)
10.1	0.294(6)	1.187(4)	1.077(8)	2.80(1)	100(0)	–	–	0(0)
11.0	0.281(5)	1.195(4)	1.060(7)	2.66(2)	100(0)	–	–	0(0)
12.0	0.275(5)	1.191(3)	1.047(5)	2.53(1)	100(0)	–	–	0(0)
13.1	0.304(6)	1.191(3)	1.024(6)	2.13(1)	100(0)	–	–	0(0)
13.5	0.319(8)	1.203(4)	1.007(8)	1.83(2)	100(0)	–	–	0(0)
13.63	0.279(6)	1.186(2)	1.004(5)	1.84(2)	72(8)	0.96(1)	0.70(5)	28(8)
13.72	0.296(23)	1.190(4)	1.015(9)	1.81(6)	62(8)	0.95(1)	0.64(8)	38(8)
14.0	0.34(3)	1.186(2)	1.022(12)	1.65(9)	28(8)	0.974(4)	0.32(2)	72(8)
14.2	0.34(6)	1.084(3)	1.035(40)	1.800(0)	17(10)	0.961(5)	0(0)	83(10)
15.0	0.244(7)	1.190(4)	0.971(8)	0.0(0)	100(0)	–	–	0(0)
15.5	0.249(7)	1.190(3)	0.963(8)	0.0(0)	100(0)	–	–	0(0)
16	0.258(3)	1.191(1)	0.970(3)	0.0(0)	100(0)	–	–	0(0)

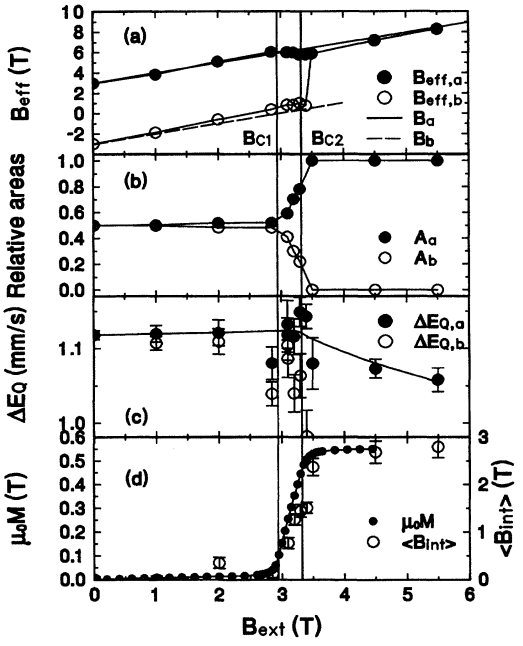

FIG. 6. Results for the spectra for $T=4.2$ K, parallel field. (a) The effective hyperfine fields $B_{\mathrm{eff},a}$ and $B_{\mathrm{eff},b}$: the lines $B_a=B_{\mathrm{eff},a}$ (4.2 K, 0 T) $+B_{\mathrm{ext}}$ and $B_b=B_{\mathrm{eff},b}$ (4.2 K, 0 T) $+B_{\mathrm{ext}}$ are shown. The starting field B_{C1} and ending field B_{C2} of the metamagnetic transition from Ref. 7 are shown as well. (b) The areas A_a and A_b. (c) The EFG $\Delta E_{Q,a}$ and $\Delta E_{Q,b}$ are shown. (d) The bulk $\mu_0 M$ from Ref. 7 is compared with the local magnetization $B_{\mathrm{eff},a}A_a+B_{\mathrm{eff},b}A_b$. Lines are guides for the eye.

(4)]. This is confirmed by the high-field results above the metamagnetic transition where only one subspectrum can be observed, and B_{eff} increases with increasing B_{ext}. Thus at lower fields, $B_{\mathrm{eff},b}<0$ corresponds to the antiparallel (denoted $-$) magnetic sublattice (as long as the subspectra areas remain equal, which they do at lower fields, see below). This metamagnetic transition is seen in Fig. 6(b), which shows the relative areas of the (a) and (b) subspectra, A_a and A_b (where $A_a+A_b=1$). Below $B_{\mathrm{ext}}=3$ T, these remain equal to 0.5. Above $B_{\mathrm{ext}}=3$ T, A_a increases from 0.5 to 1.0, while A_b decreases from 0.5 to 0. At the same time, the hyperfine fields shown in Fig. 6(a) show only a very small change. This is consistent with the mixed phase region of the metamagnetic transition: both AF- and FM-oriented regions coexist in the sample. Due to the sample shape (flat disk in a field parallel to the disk axis), the first-order metamagnetic transition at the critical field H_C is spread out over a range of (external) fields from B_{C1} to B_{C2}. The values given in Fig. 6 are taken from Ref. 7 and agree with a simple model of the metamagnetic transition: $\mu_0 M/(B_{C2}-B_{C1})=1/N_D$ (N_D is the effective demagnetizing coefficient), and the critical (external) field is $B_C\approx B_{C1}$ ($H_C=H_{C1}-N_D M\approx H_{C1}$). The small deviations in $B_{\mathrm{eff},a}$ and $B_{\mathrm{eff},b}$ from B_a and B_b in this region can be explained by the changes in the dipolar fields in the (however unknown) domain structure. The changes in area given in Fig. 6(b) show that the transition is discontinuous and occurs by spin-flip reorientations of 180°. No spin-flop reorientations of 90° were found. The effective angle as determined from the spectra, Θ_{eff}, was always fixed at zero for the fits presented, but could be easily distinguished from 90° (note that 0° and 180° orientations are distinguishable in the Mössbauer spectra only by the value of B_{eff}; otherwise Θ and $180°-\Theta$ yield the same line intensities).

The variation in the quadrupole splitting ΔE_Q (4.2 K, B_{ext}) are shown in Fig. 6(c). Below the start of the metamagnetic transition both subspectra (a) and (b) yield essentially the same value of ΔE_Q. Above the end of the transition, only one subspectrum is seen. Only within the mixed-phase region of the metamagnetic transition do we observe different values, with $\Delta E_{Q,b}<\Delta E_{Q,a}$. In addition, there is also a clear tendency for the ΔE_Q to decrease between the zero-field AF and high-field SPM states.

The metamagnetic transition is complete at $B_{\mathrm{ext}}\approx 3.5$ T [Fig. 6(a)]. Above this field, the magnetic state is described as saturated paramagnetic (SPM). From Fig. 6(a) we see that just above this field, the (single) B_{eff} lies just below the extrapolation $B_a=B_{\mathrm{eff},a}$ (4.2 K, 0 T) $+B_{\mathrm{ext}}$. This has been seen previously by Simkin.[30] It was explained as being due to the change in the dipole fields in the FM-oriented SPM state with finite magnetization M. The appropriate total dipole field is given by $B_D=-(2/3)\mu_0 M+B_3$. This has been estimated by Simkin as a change of -0.67 T between the AF and FM orientations, and agrees with the results just at the upper end of the metamagnetic transition. However, for larger external fields (not measured by Simkin), B_{eff} rejoins B_a, as seen in Fig. 6(a). This result was completely unexpected, and prompted us to redo the calculation of the total dipole field given above. Using the experimental values for the lattice constants a and c, and $g_\parallel=3.95$, we obtain the saturation magnetization in the SPM (or hypothetical ferromagnetic) state of $M_S=0.490$ MA/m, or $\mu_0 M_S=0.616$ T. This value is consistent with the measured magnetization at $T=4.2$ K, for $B_{\mathrm{ext}}\geq 6$ T, far above the metamagnetic transition.[1] For the AF state, we find $-(2/3)\mu_0 M^{(\mathrm{AF})}=0$ T, and $B_3^{(\mathrm{AF})}=-0.595$ T. For the FM state (SPM), we find $-(2/3)\mu_0 M^{(\mathrm{FM})}=-0.411$ T, and $B_3^{(\mathrm{FM})}=-0.310$ T. This results in dipole fields $B_D^{(\mathrm{AF})}=-0.595$ T, and $B_D^{(\mathrm{FM})}=-0.721$ T, or a difference in the metamagnetic transition of -0.126 T, rather than the value given by Simkin of -0.68 T. It seems that one of the terms was forgotten in the work of Simkin. Our result shows that the dipole field is a small effect in the metamagnetic transition when comparing the starting and ending homogeneously magnetized AF and FM states. We find at the highest external fields available to us a difference between B_{eff} (4.2 K, 5.5 T) and the extrapolation B_a of about 0.2 T, in good agreement with the above prediction. It must also be understood that the predictions for the dipole fields depend as well on the point charge calculations.

The local magnetization can be calculated from the hyperfine fields and relative areas for the two subspectra (a) and (b). In Fig. 6(d) we compare the weighted average of the internal field $\langle B_{\mathrm{int}}\rangle=B_{\mathrm{eff},a}A_a+B_{\mathrm{eff},b}A_b-B_{\mathrm{ext}}$ (where $A_a+A_b=1$, and $B_{\mathrm{eff},b}<0$) with the magnetization M measured in a similar sample (demagnetization constant ≈ 1). The average $\langle B_{\mathrm{int}}\rangle$ is, neglecting the (small) dipole effect, proportional to the average local magnetization. It is clear that the agreement between these two measures of the magnetization is very good. Thus we are able to reproduce the

TABLE III. Results for $T=4.2$ K, external magnetic field B_{ext} parallel to the c axis. Errors are given in parentheses [(0) denotes fixed value].

B_{ext} (T)	$\Delta E_{Q,a}$ (mm/s)	$B_{eff,a}$ (T)	A_a (%)	$\Delta E_{Q,b}$ (mm/s)	$B_{eff,b}$ (T)	A_b (%)
0.00	1.12(1)	2.99(1)	50(1)	1.12(1)	−2.99(1)	50(1)
1.00	1.12(1)	3.84(1)	50(1)	1.11(1)	−1.87(1)	50(1)
2.00	1.12(1)	5.08(1)	51(1)	1.09(1)	−0.60(1)	49(1)
2.85	1.08(1)	6.05(1)	52(1)	1.04(1)	−0.36(1)	48(1)
3.10	1.13(1)	6.05(1)	58(1)	1.08(1)	0.85(1)	42(1)
3.20	1.13(1)	5.97(1)	70(1)	1.06(1)	0.78(1)	30(1)
3.30	1.13(1)	5.83(1)	77(1)	1.04(1)	0.72(1)	23(1)
3.40	1.14(1)	5.76(1)	80(1)	1.10(1)	0.92(1)	20(1)
3.50	1.08(1)	5.87(1)	100(0)	–	–	0(0)
4.50	1.07(1)	7.18(1)	100(0)	–	–	0(0)
5.50	1.06(1)	8.30(1)	100(0)	–	–	0(0)

macroscopic properties of the transition, justifying our assumption in the fits that the sublattice (subspectrum) magnetization is parallel to the c axis. The results for the metamagnetic transition in parallel field are summarized in Table III.

3. *Results for T=4.2 and 7.0 K in perpendicular external field: Magnetic and hyperfine anisotropy*

The spectra taken in external magnetic field perpendicular to the c axis are shown in Figs. 7(a) for $T=4.2$ K, and 7(b) for $T=7.0$ K. For this case there is no distinction between the two sublattices. In addition to the effective hyperfine field B_{eff}, we now evaluate the spectra for the angle Θ_{eff}. The geometry is shown in Fig. 8. Dipole fields are calculated with respect to the positive (+) sublattice, shown schematically in Fig. 8(a). The results up to $B_{ext}=5.5$ T do not show complete saturation, as $\Theta_{eff}<90°$, so that we must extrapolate to find the hyperfine constant in the perpendicular case. We must relate the measured B_{eff} and Θ_{eff}, the known B_{ext}, the calculated dipole correction B_D, and the resulting direction and magnitude of the magnetic moments μ_{Fe} and Θ_μ. In the case of anisotropy in the hyperfine constant, μ_{Fe} and the resulting internal hyperfine field B_{hf} will no longer be parallel. We want to determine the anisotropy of the hyperfine tensor $\tilde{A}_{hf}$ for parallel and perpendicular orientations. Because of the anisotropy of the g factor given above, Eq. (2a), the Fe moment μ_{Fe} depends on Θ_μ (see Fig. 8). We assume the expression given above for the angular dependence of the magnetic moments. In addition, we use the value $g_\perp/g_\parallel=0.830$ and $g_\parallel=3.95$ for $\delta/\lambda=1$ from Eq. (2a) and the saturation magnetization in the SPM state of $M_S=0.490$ MA/m. The parallel hyperfine constant $a_{hf\parallel}$ can be obtained from the results for $T=4.2$ K in zero field: $B_{eff}(T,0)=2.99\ \text{T}=B_{hf}(T,0)+B_D(T,0)$. The dipole field estimated from Eq. (9) is $B_D^{(AF)}=-0.595$ T. This results in $a_{hf\parallel}=B_{hf}/g_\parallel\mu_B=+0.91(1)\ \text{T}/\mu_B$. The positive sign indicates that for the parallel component, the hyperfine field is parallel rather than antiparallel to the moment.

The conversion from the measured quantities B_{eff} at angle Θ_{eff} to the desired B_{hf} at angle Θ_{hf} and μ_{Fe} at angle Θ_μ is given by (see Fig. 8)

$$\begin{pmatrix} B_{eff\perp}-B_{ext} \\ B_{eff\parallel} \end{pmatrix} = \begin{pmatrix} B_{int\perp} \\ B_{int\parallel} \end{pmatrix} = \begin{pmatrix} B_{hf\perp}+B_{D\perp} \\ B_{hf\parallel}+B_{D\parallel} \end{pmatrix}. \quad (15)$$

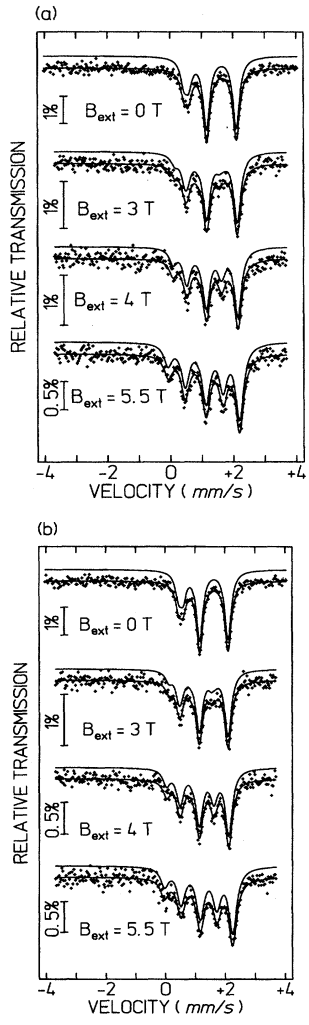

FIG. 7. Mössbauer spectra for external magnetic field perpendicular to the c axis: (a) $T=4.2$ K; (b) $T=7.0$ K. Due to symmetry, there can only be one subspectrum. The rotation of B_{eff} with increasing B_{ext} is demonstrated by the increasing line intensitiy especially near about 1.7 mm/s.

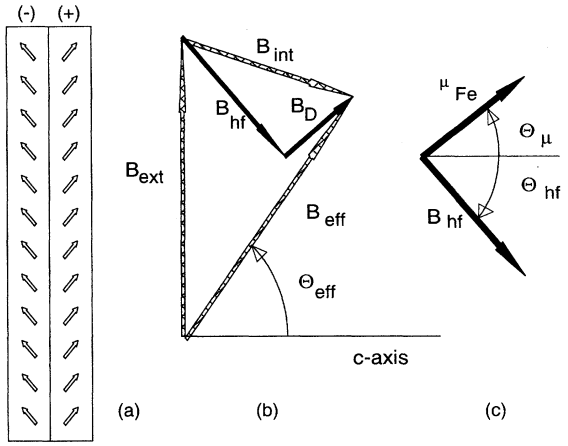

FIG. 8. Geometry of the magnetic-field vector relationships for B_{ext} perpendicular to the c axis: (a) schematic of the (+) and (−) sublattices, defined with respect to the positive c-axis direction; (b) vector relationships $B_{eff}=B_{int}+B_{ext}$, and $B_{int}=B_{hf}+B_D$; (c) due to the asymmetry of the hyperfine tensor, the hyperfine field B_{hf} can be noncollinear to the magnetic moments μ_{Fe} [shown is a moment from the (+) sublattice].

The hyperfine field vector is given by the product of the hyperfine tensor and the moment vector [see Eq. (5)]:

$$\begin{pmatrix} B_{hf\perp} \\ B_{hf\parallel} \end{pmatrix} = \mu_B \begin{pmatrix} a_\perp g_\perp \sin\Theta_\mu \\ a_\parallel g_\parallel \cos\Theta_\mu \end{pmatrix}. \tag{16}$$

We now express the resulting magnetization $\vec{M}$ for the spin texture given in Fig. 8: $\Theta_\mu^{(+)}=180°-\Theta_\mu^{(-)}=\Theta_\mu$, and obtain for the macroscopic fields $\vec{B}_1+\vec{B}_2$:

$$\vec{B}_1+\vec{B}_2=\frac{1}{3}\mu_0\mu_B\frac{N}{V}\begin{pmatrix} g_\perp \sin\Theta_\mu \\ 0 \end{pmatrix}. \tag{17}$$

The component $\vec{B}_3$ is given by

$$\vec{B}_3=\frac{1}{4\pi}\mu_0\mu_B\frac{N}{V}\begin{pmatrix} 3.17 g_\perp \sin\Theta_\mu \\ -12.18 g_\parallel \cos\Theta_\mu \end{pmatrix}. \tag{18}$$

We now consider the parallel components $B_{eff\parallel}=B_{int\parallel}=B_{hf\parallel}+B_{D\parallel}$. The latter two both involve the same factor of $\cos\Theta_\mu$. The prefactors are the zero-external-field values $B_{hf}(T,0)$ and $B_D(T,0)$ where $B_{hf}(T,0)+B_D(T,0)=B_{eff}(T,0)$, giving an expression from which we can determine Θ_μ:

$$\frac{B_{int\parallel}(T,B_{ext})}{B_{eff}(T,0)}=\cos\Theta_\mu. \tag{19}$$

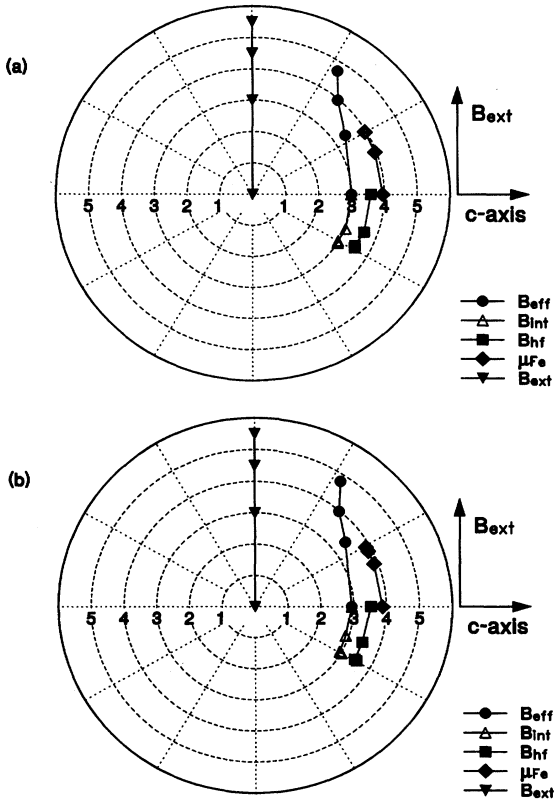

FIG. 9. Polar diagram for the hyperfine fields in the perpendicular orientation: (a) $T=4.2$ K; (b) $T=7.0$ K. These show the rotation of the hyperfine field B_{hf} in the opposite direction to μ_{Fe}.

From this, the perpendicular components $B_{D\perp}$ and $B_{hf\perp}$ have been calculated. The hyperfine constants are given by $a_{hf\parallel}=B_{hf\parallel}/(\mu_B g_\parallel \cos\Theta_\mu)$ and $a_{hf\perp}=B_{hf\perp}/(\mu_B g_\perp \sin\Theta_\mu)$. The resulting values are given in Table IV for $T=4.2$ K. Surprisingly, we obtain a negative coefficient for the perpendicular component $a_{hf\perp}\approx -0.86(4)$ T/μ_B. This difference in sign from the parallel component $a_{hf\parallel}\approx +0.91(1)$ T/μ_B results from the negative values for the perpendicular components of the internal field B_{int} and is due to changes induced in the (negative) dipole B_d and orbital B_o contributions in this orientation. This also means that the hyperfine field turns in the opposite direction than the magnetic moments in field. This is summarized in a polar diagram given in Fig. 9(a) for the results at $T=4.2$ K and Fig. 9(b) for $T=7.0$ K, showing that the hyperfine field rotates in the opposite sense to that of the moments. It is important to realize that this result shows the sensitivity of the experiment to static moments noncollinear

TABLE IV. Results for $T=4.2$ K, external magnetic field B_{ext} perpendicular to the c axis. Errors are given in parentheses [(0) denotes fixed value].

B_{ext} (T)	ΔE_Q (mm/s)	B_{eff} (T)	Θ_{eff} (deg)	Θ_μ (deg)	Θ_{hf} (deg)	$a_{hf\perp}$ (T/μ_B)
0.00	1.11(1)	2.99(1)	0(0)	0(0)	0(0)	–
3.00	1.10(1)	3.39(5)	34(2)	19.8	−19.4	−0.91
4.50	1.04(2)	3.97(10)	49(2)	30.0	−29.2	−0.83
5.50	1.07(1)	4.71(7)	57(1)	31.0	−29.5	−0.86

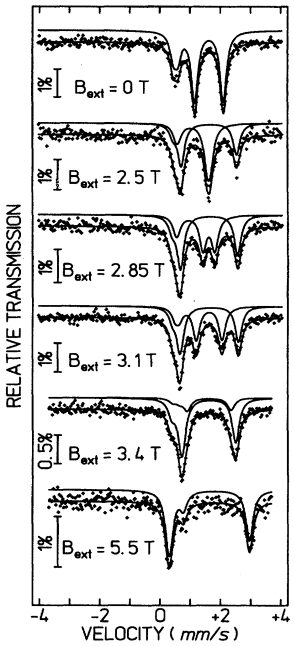

FIG. 10. Mössbauer spectra for $T=7.0$ K, external field parallel to c axis showing the two-subspectra fits.

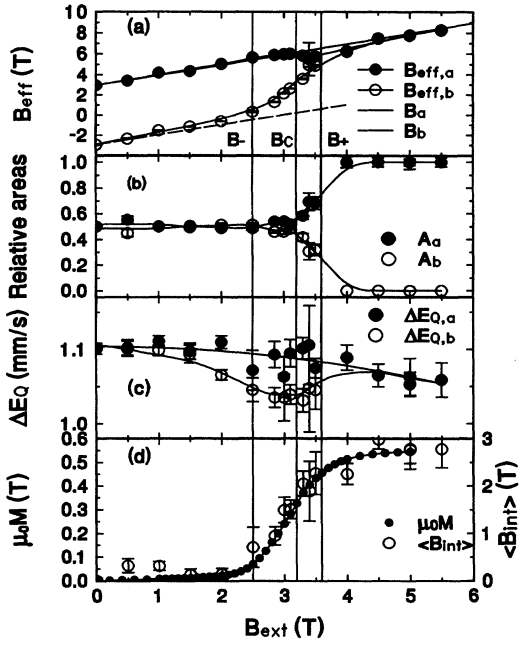

FIG. 11. Results for the spectra for $T=7.0$ K, parallel field. (a) The effective hyperfine fields $B_{\mathrm{eff},a}$ and $B_{\mathrm{eff},b}$: the lines $B_a=B_{\mathrm{eff},a}$ (7 K, 0 T) $+B_{\mathrm{ext}}$ and $B_b=B_{\mathrm{eff},b}$ (7 K, 0 T) $+B_{\mathrm{ext}}$ are shown. The lower field B_- and upper field B_+ denoting the maxima in the imaginary component of the ac susceptibility from Ref. 7 as discussed in the text are shown as well. (b) The areas A_a and A_b. (c) The EFG $\Delta E_{Q,a}$ and $\Delta E_{Q,b}$ are shown. (d) The bulk $\mu_0 M$ from Ref. 7 is compared with the local magnetization $B_{\mathrm{eff},a}A_a + B_{\mathrm{eff},b}A_b$. Lines are guides for the eye.

with the c axis, and thus it is possible to determine the spin structure by this method.

4. Results for T=7.0 and 10.1 K in parallel external field: The continuous second-order transition

The goal that we set for the Mössbauer studies was the detection of possible spin structures noncollinear with the c axis in the regions of strong noncritical fluctuations. The spectra at $T=7.0$ K are shown in Fig. 10 for different external fields parallel to the c axis. This temperature is above the MCP temperature discussed above, and the transition in field should be of second order and continuous from the AF to the SPM states at a field $H_C=2.6$ MA/m (an external field of $B=3.2$ T). The upper two spectra show qualitatively similar results as at $T=4.2$ K: the single spectrum splits into two subspectra of equal area and effective hyperfine fields shifted by the external field. For larger external fields, there are strong changes. This is best seen in Fig. 11(a) for the resulting effective hyperfine fields $B_{\mathrm{eff},a}$ and $B_{\mathrm{eff},b}$ (where as before the first is positive and the second negative for small fields). The figure also shows the branches $B_a=B_{\mathrm{eff},a}$(7 K, 0 T) $+B_{\mathrm{ext}}$ and $B_b=B_{\mathrm{eff},b}$(7 K, 0 T) $+B_{\mathrm{ext}}$ where $B_{\mathrm{eff},b}$ is negative, and the branches represent simply the shifts caused by an external field collinear with the internal field B_{int} [parallel for subspectrum (a), antiparallel for (b)]. Above an external field of B_{ext} of about 2 to 2.5 T, there is now a continuous evolution of $B_{\mathrm{eff},b}$ towards positive values, while $B_{\mathrm{eff},a}$ remains on the line B_a. This is qualitatively different than the case in the metamagnetic transition, and proves the continuous nature of the transition in this region.

The variation of the subspectra relative areas A_a and A_b are shown in Fig. 11(b). In contrast to the case for the metamagnetic transition, here the variation from equal areas of 0.5 starts at a higher field than the transition itself. In the range where the $B_{\mathrm{eff},b}$ starts to change, 2 to 2.5 T, both the relative areas A_a and A_b remain constant at 0.5. In this case, it is mainly the change in the subspectrum effective hyperfine field which indicates the transition. In the spectra taken in this region, we have never been able to find line intensities indicating a nonaxial effective hyperfine field: Θ_{eff} is either 0° or 180° for both subspectra to within our accuracy ($\pm 15°$) and time scale. (The appropriate time scale is given by the Larmor precession time of the ground-state nucleus in the total field, and this is on the order of MHz.) Although the results for the anisotropy of the hyperfine tensor given above are very unusual, it does show that perpendicular components of the magnetic moment can be measured. If we assume on the contrary a static Fe moment that changes mainly in direction Θ_μ, and minor changes in length only due to $g_\perp/g_\parallel$, then we can relate this rotation to a possible $B_{\mathrm{eff},b}$ and $\Theta_{\mathrm{eff},b}$. In this case, $B_{\mathrm{eff},b}$ can also vary continuously from the negative to the positive branch with, however, essentially fixed moment magnitude. However, the effective angle $\Theta_{\mathrm{eff},b}$ must then go through 90°, and such large angles can definitely be ruled out from the spectra. We must then conclude that the hyperfine field $B_{\mathrm{hf},b}$ varies also in a continuous way from negative to positive values, but remains collinear with the c axis. There is even a small region where $B_{\mathrm{eff},b}$ is positive, but smaller than $B_{\mathrm{eff},a}$.

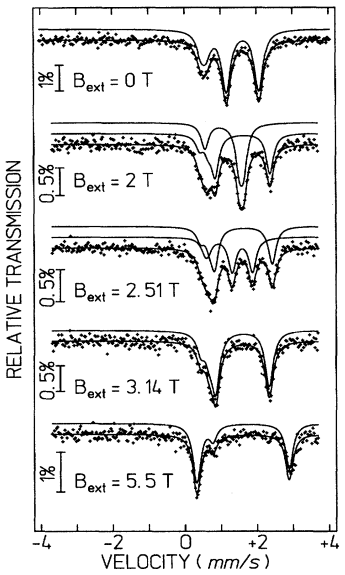

FIG. 12. Spectra for $T=10.1$ K, external field parallel to c axis showing the two-subspectra fits.

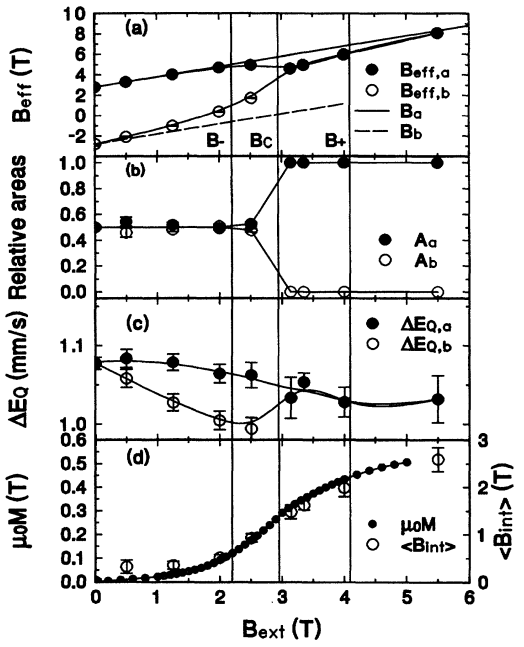

FIG. 13. Results for the spectra for $T=10.1$ K, parallel field. (a) The effective hyperfine fields $B_{\mathrm{eff},a}$ and $B_{\mathrm{eff},b}$: the lines $B_a=B_{\mathrm{eff},a}(10.1\ \mathrm{K},\ 0\ \mathrm{T})+B_{\mathrm{ext}}$ and $B_b=B_{\mathrm{eff},b}$ (10.1 K, 0 T) $+B_{\mathrm{ext}}$ are shown. The lower field B_- and upper field B_+ denoting the maxima in the imaginary component of the ac susceptibility from Ref. 7 as discussed in the text are shown as well. (b) The areas A_a and A_b. (c) The EFG $\Delta E_{Q,a}$ and $\Delta E_{Q,b}$ are shown. (d) The bulk $\mu_0 M$ from Ref. 7 is compared with the local magnetization $B_{\mathrm{eff},a}A_a+B_{\mathrm{eff},b}A_b$. Lines are guides for the eye.

The variation in the quadrupole splitting $\Delta E_Q(7.0\ \mathrm{K}, B_{\mathrm{ext}})$ for the two subspectra are shown in Fig. 11(c). Below the start of the continuous transition both subspectra (a) and (b) yield essentially the same value of ΔE_Q as was the case for $T=4.2$ K. Above the end of the transition, only one subspectrum is seen. Only within the mixed-phase region of the transition do we observe different values, with $\Delta E_{Q,b}<\Delta E_{Q,a}$. This effect is of about 0.06/1.1 or about 6%. In addition, there is also a clear tendency for the ΔE_Q to decrease between the zero-field AF and high-field SPM states of about 0.04/1.1 or 4%, between $B_{\mathrm{ext}}=0$ and 5.5 T. In the region where B_{eff} of subspectrum (b) approaches that of (a), there seems to be in addition, an effect on the field of the parallel subspectrum (a), which decreases slightly, before the fields both approach the extension to the first line along B_{eff} (7 K, 0 T) $+B_{\mathrm{ext}}$. As was the case for the metamagnetic transition, there is no offset at this point.

The local magnetization can be calculated from the hyperfine fields and relative areas for the two subspectra as in the case of the metamagnetic transition. In Fig. 11(d) we compare $\langle B_{\mathrm{int}}\rangle=B_{\mathrm{eff},a}A_a+B_{\mathrm{eff},b}A_b-B_{\mathrm{ext}}$ (where $A_a+A_b=1$, and $B_{\mathrm{eff},b}<0$) with the magnetization measured in a similar sample (same sample as for $T=4.2$ K reported on in Ref. 7). It is clear that the agreement is again very good.

The spectra for $T=10.1$ K (shown in Fig. 12) lead to the same conclusions as for $T=7.0$ K. The resulting fields and areas are given in Figs. 13(a) through 13(d). This shows the properties given above are characteristic of the continuous transition. The results for the continuous transition for $T=7.0$ K are given in Table V.

V. DISCUSSION OF RESULTS

The spectra at zero field at increasing temperature show the expected decrease in the effective hyperfine field $B_{\mathrm{eff}}(T)$ (Figs. 2 and 3). Near the Néel temperature $T_N=14.2$ K, they show in addition the superposition of two different subspectra with very different values of $B_{\mathrm{eff}}(T)$ and EFG effect $\Delta E_Q(T)$. It is known from the studies of Fujita, Ito, and Ôno[34] that the ground-state splitting D between $m_S=\pm 1$ and $m_S=0$ is about 13 K, so that in the range from $T_{\mathrm{MCP}}=4.64$ K to T_N, the thermal population in the upper state increases and the EFG splitting will be influenced by thermal fluctuations. If the relaxation time is slow enough, we should see this $m_S=0$ as a separate state. Thus we would expect to see two states, one with the maximum values of B_{eff} and ΔE_Q, and one with $B_{\mathrm{eff}}=0$, and ΔE_Q equal to the nonmagnetic value (just above T_N). This is not exactly what is observed, but it is in the correct direction. Actually, if the relaxation time of the fluctuations is near to that of the Larmor precession time of the ground-state nucleus, we should see a relaxation-type spectrum. This might be a more accurate characterization of the spectra for $T\approx T_N$. In zero external field, these fluctuations are symmetric on the two sublattices. This will no longer be the case in field, where the antiparallel sublattice will be destabilized. The magnetization process induced by the field is different for $T<T_{\mathrm{MCP}}$ and $T>T_{\mathrm{MCP}}$.

The metamagnetic phase transition in field and tricritical point have received extensive treatment in the literature, but studies of the separate sublattice magnetization have not often been reported. We have seen that the field-induced magnetization can be calculated from the results for the hyperfine

TABLE V. Results for $T=7.0$ K, external magnetic field B_{ext} parallel to the c axis. Errors are given in parentheses [(0) denotes fixed value].

B_{ext} (T)	$\Delta E_{Q,a}$ (mm/s)	$B_{eff,a}$ (T)	A_a (%)	$\Delta E_{Q,b}$ (mm/s)	$B_{eff,b}$ (T)	A_b (%)
0.0	1.10(1)	2.94(1)	50(0)	1.10(1)	−2.94(1)	50(0)
0.5	1.10(1)	3.39(1)	55(5)	1.10(1)	−2.35(1)	45(5)
1.0	1.11(1)	4.18(1)	50(1)	1.10(1)	−1.54(1)	50(1)
1.5	1.10(1)	4.43(1)	51(1)	1.09(1)	−1.15(1)	49(1)
2.0	1.11(1)	5.05(1)	49(1)	1.06(1)	−0.62(1)	51(1)
2.5	1.07(1)	5.66(1)	49(1)	1.04(1)	0.32(1)	51(1)
2.85	1.09(1)	5.91(1)	54(1)	1.03(1)	1.30(1)	46(1)
3.0	1.06(1)	5.95(1)	54(1)	1.03(1)	2.14(1)	46(1)
3.1	1.09(1)	6.02(1)	52(1)	1.04(1)	2.63(1)	48(1)
3.3	1.10(1)	5.83(1)	58(1)	1.03(1)	3.59(1)	42(1)
3.4	1.10(1)	5.49(1)	69(1)	1.08(1)	4.95(1)	31(1)
3.5	1.08(1)	5.77(1)	68(1)	1.06(1)	4.91(1)	32(1)
4.0	1.09(1)	6.25(1)	100(0)	–	–	0(0)
4.5	1.06(1)	7.48(1)	100(0)	–	–	0(0)
5.0	1.06(1)	7.79(1)	100(0)	–	–	0(0)
5.0	1.05(1)	7.77(1)	100.(0)	–	–	0.(0)
5.5	1.06(1)	8.28(1)	100.(0)	–	–	0.(0)

fields and areas of the two subspectra seen in external field. This is shown both in the metamagnetic region (Fig. 6) and the continuous transition region (Figs. 10 and 11). In addition, we now have a microscopic picture of the magnetization process, given by the effective hyperfine fields $B_{eff,a}$ and $B_{eff,b}$. The (a) and (b) subspectra can be identified with the parallel and antiparallel sublattices, as long as the subspectrum areas remains equal.

In the metamagnetic mixed phase region, the sample magnetization breaks up into regions of AF and FM orientation. This is seen in the resulting change in the relative areas of the two subspectra, with at the same time almost no change in the effective hyperfine fields. The small changes seen in Figs. 3(a) and 4(a) are understandable as changes induced in the dipole-field contribution B_D due to the changing domain structure. From Eq. (9), the contribution B_1 to the dipole field can change by about 0.5 T for a changing domain structure (the maximum change in the effective demagnetization factor is 1). In the high-field region above the transition, we have seen that the resulting dipole field is small, contrary to the results reported earlier.[30] It seems that Simkin has neglected terms in the total dipole field. This transition is spread over a range of external fields only because of the finite demagnetizing effects.

The results for the continuous second-order transition for $T>T_{MCP}$ are very different. In this case, there is a strong but continuous variation of the effective hyperfine field $B_{eff,b}$ of the antiparallel sublattice [Figs. 11(a) for $T=7.0$ K and 13(a) for $T=10.1$ K]. At the same time, no transversal components are found in the spectra. We must conclude that the smaller effective hyperfine fields are a result of the precession of the local moments around the c axis. Due to the finite time window of the measurement process, only the static component parallel to the c axis is observed. A surprising result is that this component is continuous from a maximum negative, to almost maximum positive value while at the same time being distinct from the first subspectrum (a). This means that there is a field region in which we observe two different effective hyperfine fields, and thus effective moments, and in a small region, both are positive. They join together at an effective hyperfine field slightly smaller than the linear extrapolation for the parallel subspectrum. At high external fields, the now single effective hyperfine field rejoins this extrapolation.

It is significant that the characteristic fields that we have found for the magnetizing process in the continuous region agree well with the fields characterizing the longitudinal fluctuations found in the ac susceptibility. These have been denoted H_- for the lower limit and H_+ for the upper.[7] We have given in Figs. 11(a) and 13(a) the (external) fields $B_-=\mu_0 H_-$ and $B_+=\mu_0 H_+$, which compare well with the starting and ending points of the variation of $B_{eff,b}$. At the same time, $B_{eff,a}$ changes much less. It was found from the ac susceptibility that there is a strong decrease in the *longitudinal* noncritical fluctuations for $B_-\leq B_{ext}\leq B_+$ as seen by a *local minimum* in χ'' at B_C and maxima at B_- and B_+. These properties of $B_{eff}(T,B_{ext})$ for the two subspectra are the result of the magnetic fluctuations induced by the external field. These fluctuations are seen at first as a precession of the whole antiparallel sublattice, because the relative area at first does not change but $B_{eff,b}$ deviates from the line B_b. This also shows that at first, the fluctuations are concentrated on this sublattice. With increasing field, $B_{eff,b}$ indicates a moment parallel rather than antiparallel to the external field. At the same time, the relative area of this subspectrum decreases slightly from 0.5 and the effective field on the "+" sublattice, $B_{eff,a}$, deviates slightly below B_a. This means that the fluctuations include also part of the first sublattice, but not all of it. These fluctuations persist even into the region where all the moments are at least nominally in the field direction. These results from Mössbauer spectroscopy allow a possible explanation for the novel behavior of the longitudinal spin susceptibility. In this field region, a new type of AF phase develops with canting fluctuations. This

canted but precessing structure contains $m_S=0$ spin components leading to an *increase* in the *transversal* components of the noncritical fluctuations, and a concomitant decrease in the longitudinal components. This is seen as a decrease in the imaginary component of the ac susceptibility χ'' in the region around the critical field B_C. These results qualitatively agree with recent quantum-Monte-Carlo data,[9] which predict an anomalous decrease of the staggered magnetization within $H_- \leq H \leq H_C$. Between the CE (at $T_{MCP}=4.64$ K) and the BCE (at $T \approx 5.7$ K) even a first-order transition is conjectured,[9] which, however, remains to be evidenced by future investigations.

VI. CONCLUSIONS

ac susceptibility studies[7] of the second-order continuous transition above the multicrtitical temperature T_{MCP} but below T_N have shown that in the continuous transition region the real part χ' has a maximum at the critical line in field $H_C(T)$. The results for the imaginary part χ'' as a function of T and H_a yield characteristic fields H_- below H_C, and H_+ above which denote regimes of strong noncritical fluctuations. The anomalies in the ac and total magnetization of $FeBr_2$ have been attributed to the competing interactions along the in-plane axes of the triangular Fe lattice planes.[7,8] The presence of these anomalies, and the vanishing of the imaginary part of the ac susceptibility at the critical line suggest that there are transverse in addition to the longitudinal fluctuations involved in this transition. The Mössbauer studies presented here confirm this view. Along the second-order critical line, the transition from the AF to the saturated PM states proceeds by a continuous change in the *local* moments of mainly the *antiparallel sublattice*, which vary from polarized in the negative to the positive directions but remaining parallel to the c axis. This variation is over a field range that agrees well with the characteristic fields H_- and H_+ as derived from the ac susceptibility and total magnetization[7] and from quantum-Monte-Carlo calculations.[9] It is a direct consequence of the transverse noncritical fluctuations — spin precessions — on the antiparallel sublattice induced by the external field in the presence of the competing exchange interactions.

ACKNOWLEDGMENTS

This work was supported by the SFB 166 and by the D.A.A.D.

[1] A.R. Fert, P. Carrara, M.C. Lanusse, G. Mischler, and J.P. Redoulès, J. Phys. Chem. Solids **34**, 223 (1973).
[2] J.M. Kincaid and E.G.D. Cohen, Phys. Rep. **22**, 57 (1975).
[3] M.C. Lanusse, P. Carrara, A.R. Fert, G. Mischler, and J.P. Redoulès, J. Phys. (Paris) **33**, 429 (1972).
[4] S. Pouget, Ph.D. thesis, University of Toulouse, 1994.
[5] W.B. Yelon and C. Vettier, J. Phys. C **8**, 2760 (1975).
[6] D. Bertrand (unpublished).
[7] M.M. Pereira de Azevedo, Ch. Binek, J. Kushauer, W. Kleemann, and D. Bertrand, J. Magn. Magn. Mater. **140-144**, 1557 (1995).
[8] W. Selke and S. Dasgupta, J. Magn. Magn. Mater. **147**, L245 (1995).
[9] K. Held, M. Ulmke, and D. Vollhardt (unpublished).
[10] G. Mischler, P. Carrara, and Y. Merle d'Aubigné, Phys. Rev. B **15**, 1568 (1977).
[11] M.K. Wilkinson, J.W. Cable, E.O. Wollan, and W.C. Koehler, Phys. Rev. **113**, 497 (1959).
[12] U. Balucani and A. Stasch, Phys. Rev. B **32**, 182 (1985).
[13] W.B. Yelon and C. Vettier, Solid State Commun. **15**, 391 (1974).
[14] D.J. Lockwood, in *Light Scattering in Solids*, edited by M. Cardona and G. Güntherodt (Springer-Verlag, Berlin, 1982), Vol. III.
[15] D. Petitgrand and P. Meyer, J. Phys. Paris **37**, 1417 (1976).
[16] *Advances in Mössbauer Spectroscopy*, edited by B.V. Thosar and P.K. Iyengar (Elsevier, Amsterdam, 1983).
[17] I.W. Johnstone, D.J. Lockwood, and G. Mischler, J. Phys. C **11**, 2147 (1978).
[18] R.B. Griffiths and J.C. Wheeler, Phys. Rev. A **2**, 1047 (1970).
[19] E. Stryjewski and N. Giordano, Adv. Phys. **26**, 487 (1977).
[20] J.M. Kincaid and E.G.D. Cohen, Phys. Rep. **22**, 57 (1975).
[21] F. Harbus and H.E. Stanley, Phys. Rev. **8**, 1141 (1973); **8**, 1156 (1973).
[22] L. Hernández, H.T. Diep, and D. Bertrand, Europhys. Lett. **21**, 711 (1993).
[23] I.S. Jacobs and P.E. Lawrence, J. Appl. Phys. **35**, 996 (1964).
[24] Z. Onyszkiewicz, Physica **103A**, 226 (1980); **103A**, 274 (1980); Phys. Status Solidi B **99**, K151 (1980); **122**, 543 (1984).
[25] E. Rastelli and A. Tassi, J. Phys. C **16**, 4663 (1983); J. Magn. Magn. Mater. **34**, 1041 (1983).
[26] G.C. Psaltakis, G. Mischler, D.J. Lookwood, M.G. Cottam, A. Zwick, and S. Legrand, J. Phys. C **17**, 1735 (1984).
[27] X.H. Qu and P.D. Loly, J. Phys. Condens. Matter **4**, 5419 (1992).
[28] R.J. Birgeneau, W.B. Yelon, E. Cohen, and J. Makovsky, Phys. Rev. B **5**, 2607 (1972).
[29] R.E. Watson and A.J. Freeman, Phys. Rev. **123**, 2027 (1961).
[30] D.J. Simkin, Phys. Rev. **177**, 1008 (1969).
[31] E.F. Bertaut, in *Magnetism III*, edited by G.T. Rado and H. Suhl (Academic, New York, 1963), p. 149.
[32] F. Varret, J. Phys. Chem. Solids **37**, 265 (1976).
[33] K.C. Mishra, K.J. Duff, P. Kelires, S.K. Mishra, and T.P. Das, Phys. Rev. B **32**, 58 (1985).
[34] T. Fujita, A. Ito, and K. Ôno, J. Phys. Soc. Jpn. **27**, 1143 (1969).
[35] C. Kittel, *Introduction to Solid State Physics* (Wiley, New York, 1956).
[36] J. Owen and J.M.H. Thornley, Rep. Prog. Phys. **29**, Pt. 2, 675 (1966).
[37] R. Ingalls, Phys. Rev. **133**, 787 (1964).
[38] R. Zimmermann, A. Trautwein, and F.E. Harris, Phys. Rev. B **12**, 3902 (1975).
[39] P. Gütlich, R. Link, and A. Trautwein, *Mössbauer Spectroscopy and Transition Metal Chemistry* (Springer-Verlag, Berlin, 1978).